

## Supporting Information

### Integration of a recyclable silver substrate for surface-enhanced Raman spectroscopy in digital microfluidic

Sebastian Fehse<sup>‡</sup>, Anish Das<sup>‡\*</sup>, and Detlev Belder<sup>\*</sup>

Institute of Analytical Chemistry, Leipzig University, Linnéstraße 3, D-04103 Leipzig, Germany.

‡These authors contributed equally, \* Corresponding authors

E-mail: anish.das@uni-leipzig.de and belder@uni-leipzig.de

#### Table of Contents:

	Content	Page No.
<b>S1</b>	Materials	2
<b>S2</b>	Chemical preparation	2
<b>S3</b>	Integration of TiO <sub>2</sub> thin film layer on DMF top plate	3
<b>S4</b>	Photochemical deposition of AgNP@TiO <sub>2</sub> thin film layer on DMF top plate	4
<b>S5</b>	DMF chip assembly	5
<b>S6</b>	DMF device operation	5
<b>S7</b>	SERS measurements	6
<b>S8</b>	XRD data	6
<b>S9</b>	Raman Peak assignment for methylene blue	7
<b>S10</b>	On-chip workflow for DMF-based SERS detection and recycling process	8
<b>S11</b>	Analytical enhancement factor	9
<b>S12</b>	Mechanism of the photocatalysis	10
<b>S13</b>	Control Experiment with cleaning solution	11
<b>S14</b>	Control Experiment with UV irradiation	12
<b>S15</b>	Comparison between on-chip vs off-chip AgNP@TiO <sub>2</sub> SERS substrate	13
<b>S16</b>	Droplet movement speed	14
<b>S17</b>	SERS substrate reproducibility	15
<b>S18</b>	Limit of detection (LOD)	15
<b>S19</b>	Detection-recycling cycles for malathion	16
<b>S20</b>	Trade-off between droplet movement versus SERS detection	17
<b>S21</b>	SEM image of the SERS substrate after five cycle	19

## S1. Materials

Tetrabutyltitanate (97 %), triethanolamine (98 %), malachite green chloride (MG, analytical standard), malathion (analytical standard), Teflon AF 1600 (469610-G1) and Fluorinert FC-40 (F9755) were obtained from Sigma-Aldrich Chemie GmbH (Steinheim, Germany). Silver nitrate (99.9 %) was purchased from S3 Handel und Dienstleistungen UG (Bad Oeynhausen, Germany). HPLC grade ethanol and methanol were acquired from Carl-Roth GmbH + Co.KG (Karlsruhe, Germany). Technical grade iso-propanol, acetone, acetic acid, and methylene blue (MB) were purchased from Carl-Roth GmbH + Co.KG (Karlsruhe, Germany). Ultrapure water was obtained from a Smart2Pure purification system (18.2 MΩ cm, TKA Wasseraufbereitungssysteme GmbH, Germany). All chemicals were used as received unless otherwise stated.

## S2. Chemical preparation

**TiO<sub>2</sub> precursor solution:** The protocol for preparing the TiO<sub>2</sub> precursor solution was adapted from a method reported by Zhang *et. al.*,<sup>1</sup> and modified substantially for our approach. A solution containing 289 μL DI water, 584 μL ethanol and 114 μL acetic acid was mixed together in a vial. A second solution containing 4553 μL ethanol, 1375 μL tetrabutyl titanate and 528 μL triethanolamine was mixed together and stirred for 10 min. Afterwards the first solution was added to the second solution dropwise over a period of 30 min with constant stirring. The resulting clear mixture is defined as the titanium dioxide (TiO<sub>2</sub>) precursor solution. This solution was used to prepare TiO<sub>2</sub> thin film on the DMF top plate. The solution was sealed air tight and stored in the dark in a refrigerator and used within 2-3 days.

**Silver nitrate solution:** 50 mM silver nitrate solution was prepared by dissolving 849.35 mg silver nitrate in 100 mL DI water.

**Methylene blue and malachite green solution:** A 10 mM stock solution of methylene blue (MB) was prepared by dissolving 31.99 mg methylene blue in 10 mL of DI water/ methanol (8:2 vol%). From the stock solution, 10 μM of MB working solution was prepared for each experiment. Malachite green working solution (10 μM) was also prepared similarly. 50 μM of malathion was prepared in DI water/ methanol (8:2 vol%).

**Teflon:** The hydrophobic solution was prepared by dissolving Teflon AF 1600 in Fluorinert FC-40 (1% wt/wt). For this purpose, 0.2 g of Teflon AF 1600 were mixed with 19.8 g of FC-40 in a tightly sealed vial with parafilm. The mixture was stirred with a magnetic stirrer at 300 rpm with a temperature of 40 °C on a heat plate (RSM-10HS, Phoenix Instrument, Garbsen, Germany). The result was a clear colourless slightly viscous solution. This solution was spin coated (Spin150 Manufacturer: APT GmbH, Bienenbüttel, Germany) on the DMF chip for individual experiments.

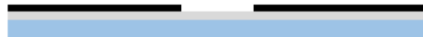
### S3. Integration of TiO<sub>2</sub> thin film layer on DMF top plate

#### Top plate

(a) ITO sputtered glass slide



(b) Adhesive mask



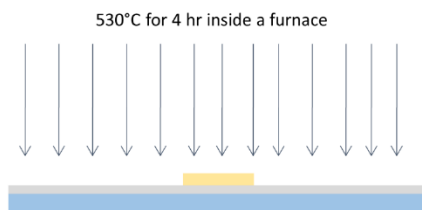
(c) Spin coating TiO<sub>2</sub> precursor



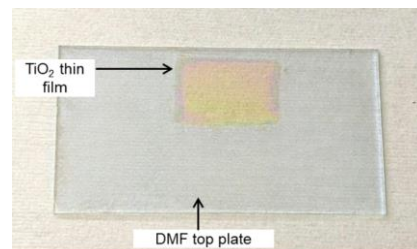
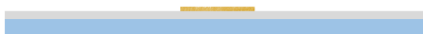
(d) Mask peel off



(e) Baking at high temperature



(f) TiO<sub>2</sub> thin film layer



■ Glass slide ■ ITO ■ Mask ■ TiO<sub>2</sub> precursor ■ TiO<sub>2</sub> thin film

**Figure 1.** Schematic side view of the chip fabrication protocol for integration of TiO<sub>2</sub> thin film layer on DMF top plate.

The ITO glass slides (fused silica, 60 x 30 x 1 mm) were cleaned with acetone, isopropanol and dried with nitrogen (Figure 1a). Before spin-coating the ITO glass, most of the surface was covered with an adhesive foil (dicing tape, Ultron Systems Inc., USA), which served as a spin-coating mask. The mask has a rectangular cutout of about 1 cm<sup>2</sup> (Figure 1b). This is where the TiO<sub>2</sub> precursor solution is deposited. The substrate was spin-coated for 60 s at 3000 rpm (Figure 1c). After removing the mask, only the rectangular area was covered with TiO<sub>2</sub> precursor solution (Figure 1d). The substrate was then annealed at 530 °C for 2 h (Figure 1e) and held at this temperature for another 2 h inside a muffle furnace

(Nabertherm GmbH, Lilienthal, Germany). The substrate was then slowly cooled to room temperature. The result was an inert, transparent and flat TiO<sub>2</sub> thin film layer on top of the ITO glass (Figure 1f).

#### S4. Photochemical deposition of AgNP@TiO<sub>2</sub> thin film layer on DMF top plate

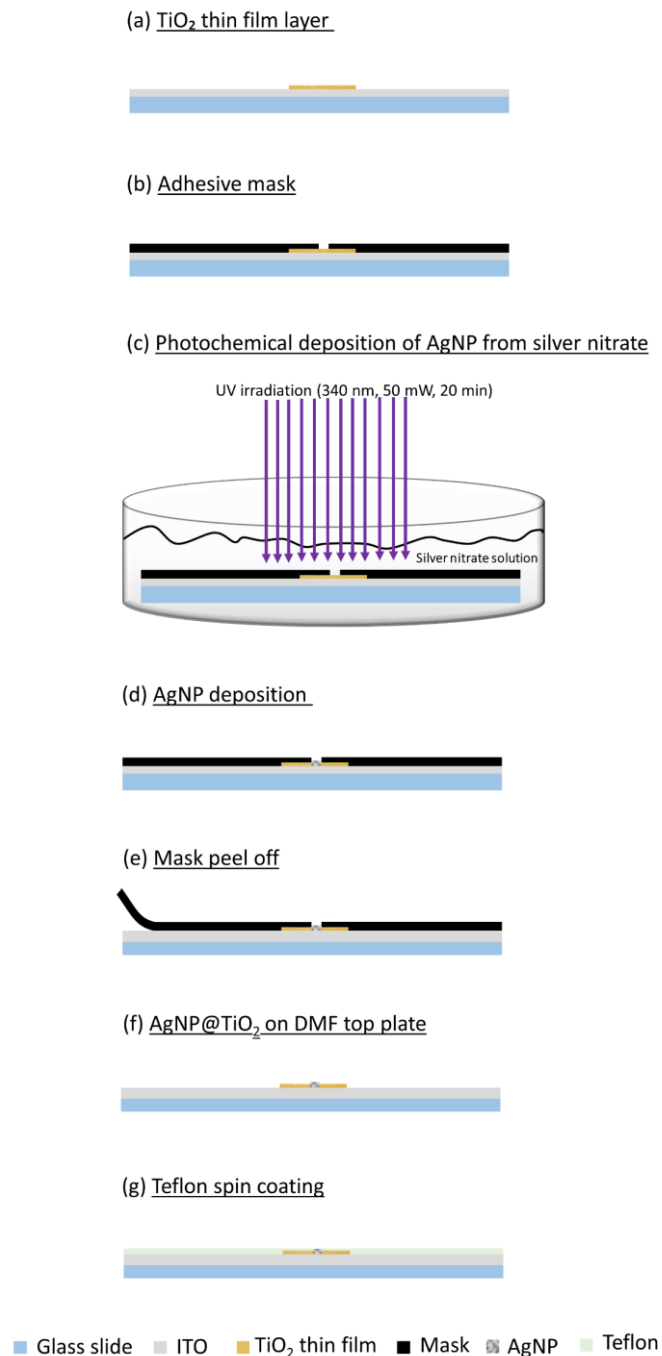


**Figure 2.** Schematic side view of the chip fabrication protocol for photochemical deposition of AgNP@TiO<sub>2</sub> thin film layer on DMF top plate.

The AgNPs were deposited on the TiO<sub>2</sub> film photochemically. The substrate with the TiO<sub>2</sub> (Figure 2a) was covered with an adhesive mask (dicing tape, Ultron Systems Inc., USA ) with a circular cutout of 1 mm diameter (Figure 2b). This is where the AgNPs will be deposited. The masked substrate was then placed in a 50 mM AgNO<sub>3</sub> solution and irradiated with UV light of 340 nm excitation wavelength and 60 mW power (M340L4, Thorlabs, Bergkirchen, Germany). The distance between the source and the substrate was approximately 1 mm. The substrate was irradiated in this manner for 20 minutes (Figure 2c). Then, the irradiated substrate was removed from the silver nitrate solution and rinsed with deionized water (Figure 2d). The adhesive mask was removed (Figure 2e), leaving a circular spot of AgNPs on the TiO<sub>2</sub> film (Figure 2f). To hydrophobize the surface, a layer of Teflon solution was spin-coated (Spin150: APT GmbH, Bienenbüttel, Germany) on the substrate for 60 s at 3000 rpm. A drop of isopropanol (1  $\mu$ L) was then used to carefully remove the Teflon solution from the SERS substrate (Figure 2g). Finally, the layer was dried at 120 °C for 4 h.

### S5. DMF chip assembly

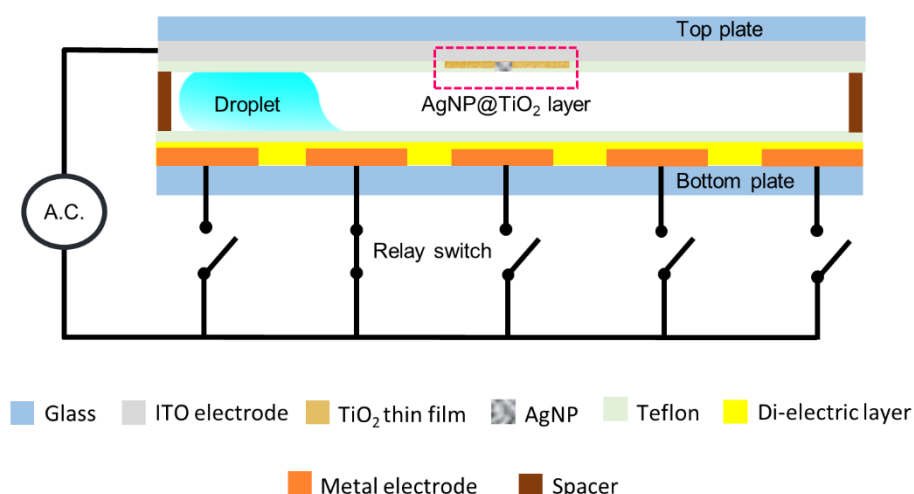


**Figure 3.** Schematic side view of the digital microfluidics chip showing the different layers.

### S6. DMF device operation

The DMF chip bottom plate consists of gold coated electrode array board (4 reservoir electrode and 124 actuation electrodes, 2.75 x 2.75 mm in size). An ethylene tetrafluoroethylene (ETFE) foil (~15  $\mu$ m, dielectric layer) coated with Teflon AF 1600 (hydrophobic layer) is laminated onto the electrode array. An ITO glass (top plate) protected with a top cover and frame, is assembled to the bottom plate using adhesive such that the inter-plate gap is ~240  $\mu$ m. The DMF droplet actuation were performed via an electric potential of 280 V<sub>p-p</sub> at 1.0-1.5 kHz applied on designated electrodes using an OpenDrop V4 system (GaudiLabs, Luzern, Switzerland). The OpenDrop V4 control system was connected to a laptop via USB-C cable and "OpenDropController" software (GaudiLabs, Luzern, Switzerland) was used to program the droplet actuation workflow. The reservoir electrodes was filled with reagent solutions, and a single unit droplet dispensed from the reservoir was around 1.46  $\pm$  0.15  $\mu$ L.

## S7. SERS measurements

The Raman spectra were acquired from a confocal modular Raman measurement setup (S&I Spectroscopy & Imaging GmbH, Warstein, Germany) fitted with a 532 nm excitation laser (Cobolt AB, Solna, Sweden) with a power of 100 mW. For Raman measurements, the sample was positioned on an upright IX71 epifluorescence upright microscope (Olympus Corporation, Tokyo Japan), which was equipped with a LUCPlanFI 40X objective (NA 0.6) (Olympus Corporation, Tokyo Japan) for focusing the laser beam onto the DMF Chip. The incident (excitation) laser power on the sample was approx. 13 mW controlled using a ND (Neutral-density) filter wheel (Thorlabs INC, NJ, USA). The scattered light passed an Andor Kymera 193i Spectrograph (Oxford Instruments, Abingdon, United Kingdom) with an entrance slit of 100  $\mu\text{m}$  and a grating of 1800 lines/mm and was detected via Andor Newton 1024 x 255 CCD camera (Oxford Instruments, Abingdon, United Kingdom). An exposure time of 1 s was used for all measurements. The spectra were collected in the range of 300 to 1900  $\text{cm}^{-1}$  with a spectral resolution of 3  $\text{cm}^{-1}$ . VistaControl V4.2 Build 12596 (S&I Spectroscopy & Imaging GmbH, Warstein, Germany) was used as interface and recording software.

## S8. XRD data

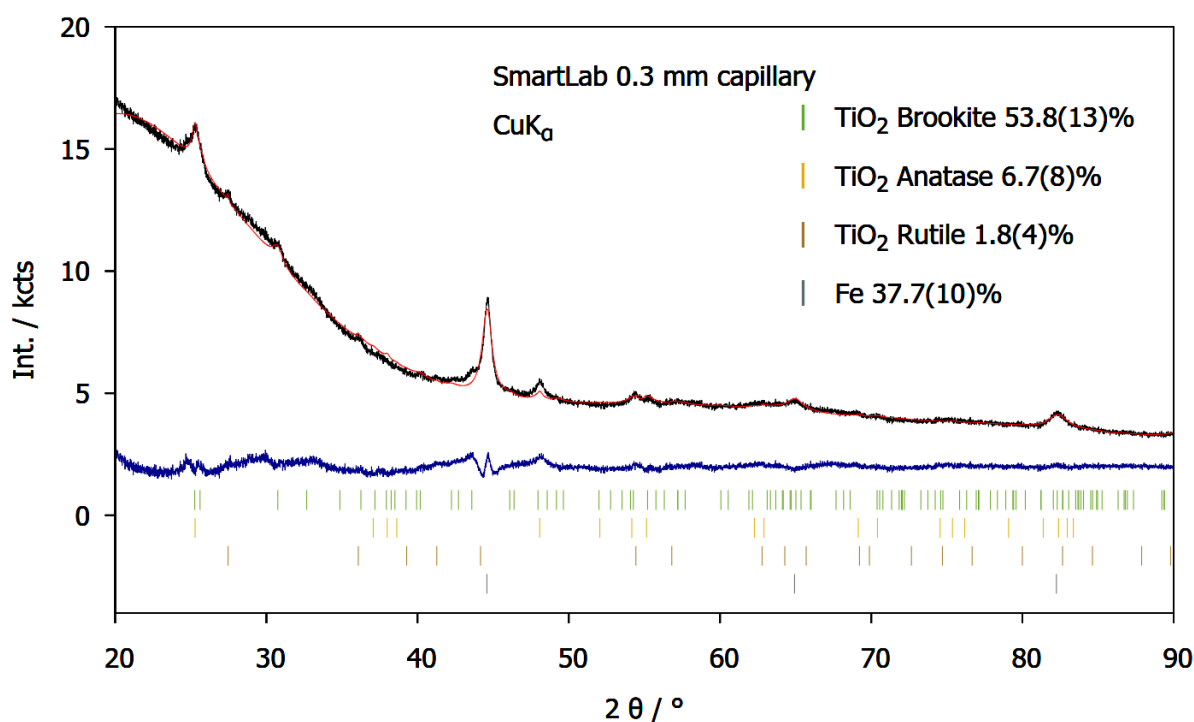
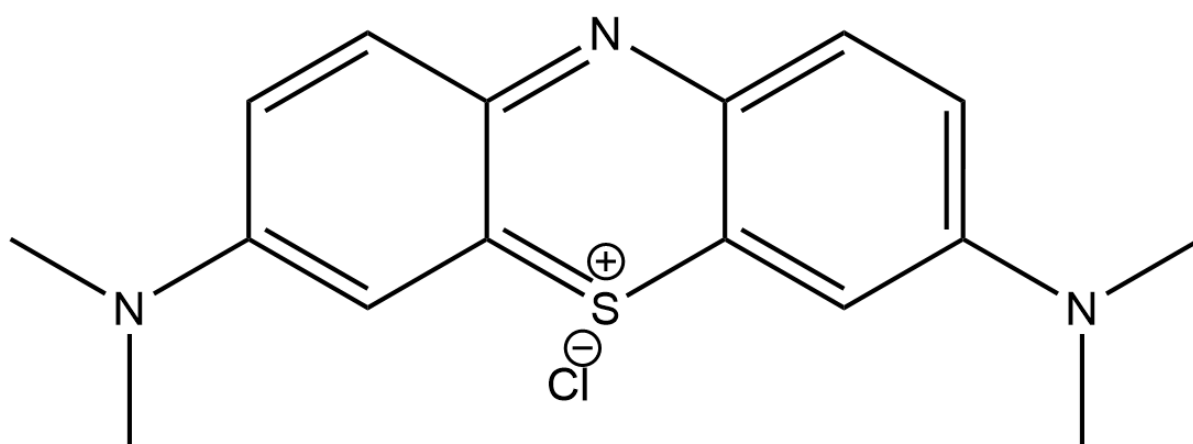


**Figure 4.** Rietveld refinement of powder XRD measurement for the fabricated titanium dioxide: - black diffractogram: measured, red diffractogram: calculated, blue: difference. The quality factors calculated by the software:  $R_{\text{exp}} = 1.25\%$ ,  $R_{\text{wp}} = 2.25\%$ ,  $R_p = 1.76\%$ , goodness of fit (GOF) = 1.80.<sup>2-5</sup>

In order to investigate the conversion of tertbutyltitanate into  $\text{TiO}_2$ , X-Ray powder diffraction was performed. A substrate with a thin layer of annealed  $\text{TiO}_2$ -precursor solution was used and the dry and hard layer was scraped off with a spatula. The thereby generated white powder was pestled and transferred into a 0.3 mm glass capillary. Rietveld analysis of the pattern was acquired using a Rigaku SmartLab diffractometer with a HyPix-3000 detector employing Cu- $\text{K}\alpha$ -radiation (Rigaku Corporation, Tokyo, Japan), was performed using the topas (ver. 5, Bruker AXS) software.<sup>6,7</sup>

The diffractogram in figure 4 shows signals for several phases of TiO<sub>2</sub> as well as iron. Supposedly the iron became part of the tested powder during the process of the scraping of the hard layer of TiO<sub>2</sub> with the spatula. Neither in the precursor solution or in the heating process iron-containing chemicals were used. Thereby the iron can be ignored. As it is shown in the graph the layer of TiO<sub>2</sub> contains different phases. Omitting the iron, the TiO<sub>2</sub> phases are made up of 87% Brookite, 11% Anatase and 2% Rutile. It has to be taken into account that the software only calculates the phase contents for the crystalline portion of the sample. Thus the layer contains amorphous and crystalline phases. The most abundant crystalline phase is brookite with 87%.

### S9. Raman peak assignment for methylene blue



Raman peak (cm <sup>-1</sup> )	Vibrational modes
448	C-N-C skeleton bending
498	C-N-C skeleton bending
596	C-S-C skeleton bending
674	C-H out-of-plane bending
774	C-H in-plane bending
894	C-H in-plane bending
956	C-H in-plane bending
1043	C-H in-plane bending
1160	C-N stretching
1310	C-H in-plane scissoring, C-H in-plane ring deformation
1400	C-H in-plane ring deformation, C-N symmetric stretching
1447	C-N antisymmetric stretching
1628	C-C ring stretching

**Figure 5.** Chemical structure and Raman peak assignment for methylene blue.<sup>8-10</sup>

## S10. On-chip workflow for DMF-based SERS detection and recycling process

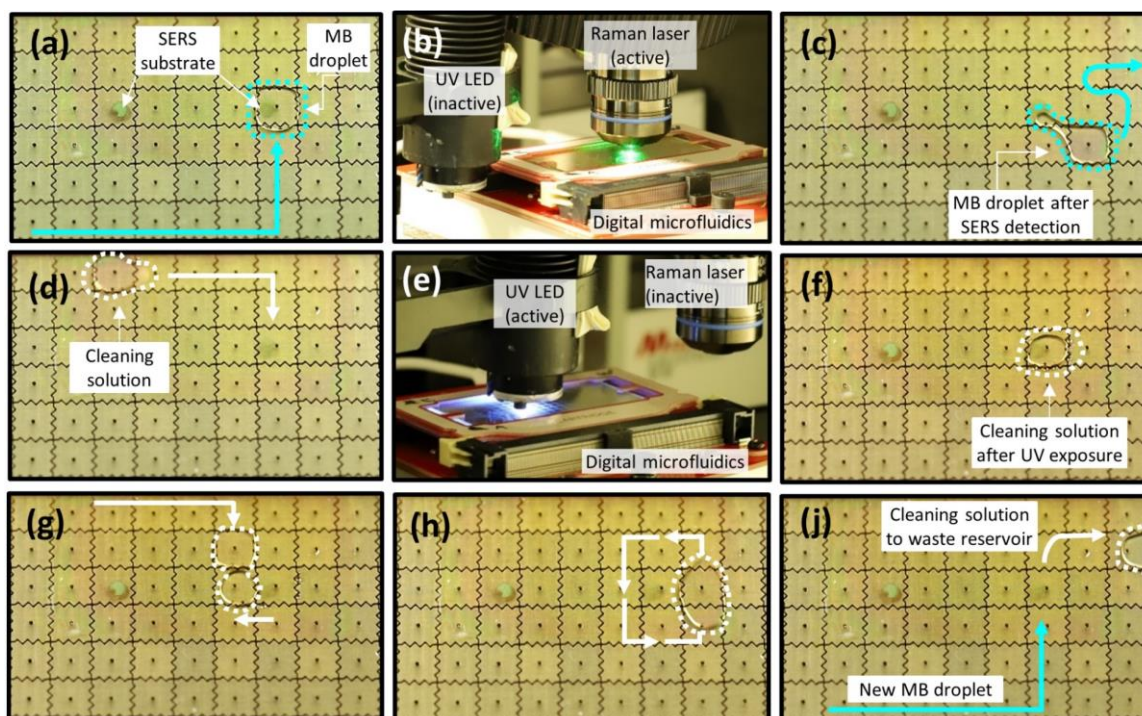


**Figure 6.** Series of images showing the droplet actuation steps inside the digital microfluidics chip integrated with the AgNP@TiO<sub>2</sub> SERS substrate for consecutive detection and recycling process. The cyan arrow indicates the MB droplet actuation direction, the white arrow indicates the cleaning solution droplet actuation direction and the dashed lines indicate the droplet boundary.

The whole DMF workflow was pre-programmed to automatically dispense MB (10  $\mu$ M) droplets from the reservoir electrode and was actuated towards the electrode underneath the SERS substrate (Fig. 6a) using electric potential of 280 Vp-p at 1.0 kHz (droplet speed: 2.75 mm s<sup>-1</sup> ( $\pm$  2.2%)). The Raman laser was activated to monitor the SERS signal of the analyte (Fig. 6b). To avoid overexposure of the AgNP@TiO<sub>2</sub> SERS substrate to laser light and ensure the acquisition of as comparable data as possible, each time the spot was limited to a maximum irradiation time of 1 min during the measuring period. After the SERS measurement, the analyte droplet could be easily moved away from the SERS substrate using EWOD forces, as evident from Fig. 6c (also step 4 in ESI<sup>+</sup> Video S1). To initiate the recycling process, a cleaning solution (DI water/methanol (8 : 2 vol%)) was dispensed from another reservoir and parked under the now-contaminated SERS substrate (Fig. 6d). Next, the UV LED (340 nm, 60 mW) irradiated the SERS substrate containing the cleaning solution for a total of 15 min (Fig. 6e). The cleaning solution was exchanged automatically every 5 min. In additional experiments, we measured the SERS spectra at every 5 min interval to determine the required recycling time. After 15 min of UV irradiation, it can be observed that the droplet shrinks to approximately half its initial volume (Fig. 6f), but this did not impede the droplet actuation, as evident from the ESI<sup>+</sup> video 1. The droplet can be moved further to the adjacent electrode using EWOD forces (Fig. 6g). Subsequently, another fresh cleaning droplet is dispensed and merged with the previous droplet to increase the droplet volume. The droplet is then circulated around the recycled SERS substrate electrode to extract any additional minute droplets formed during UV illumination (Fig. 6g, h). Subsequently, all the droplets are then transported to the waste reservoir and the recycled SERS substrate is now ready for a new detection sequence (Fig. 6j). This process was repeated several times to achieve multiple recycling and detection cycles.

## S11. Analytical enhancement factor (AEF)

In this contribution, since SERS is used for analytical applications, we calculated the analytical enhancement factor<sup>11</sup>  $AEF$ , as shown in formula 1.

$$AEF_{1628\text{ cm}^{-1}} = \frac{I_{SERS}}{I_{RS}} \cdot \frac{c_{RS}}{c_{SERS}} \quad \mathbf{1}$$

For the intensities, the peak height of MB after background correction was used.  $I_{SERS}$  refers to the SERS intensity at  $1628\text{ cm}^{-1}$ ,  $I_{RS}$  referring to the normal Raman intensity at  $1628\text{ cm}^{-1}$ ,  $c_{RS}$  refers to the concentration of the MB analyte used in normal Raman-spectroscopy and  $c_{SERS}$  referring to the concentration of MB used for SERS measurements. Conditions: Laser power- 13 mW, exposure time- 1 sec, number of accumulation-1, Droplet volume inside chip-  $\sim 1.3\text{ }\mu\text{L}$ .

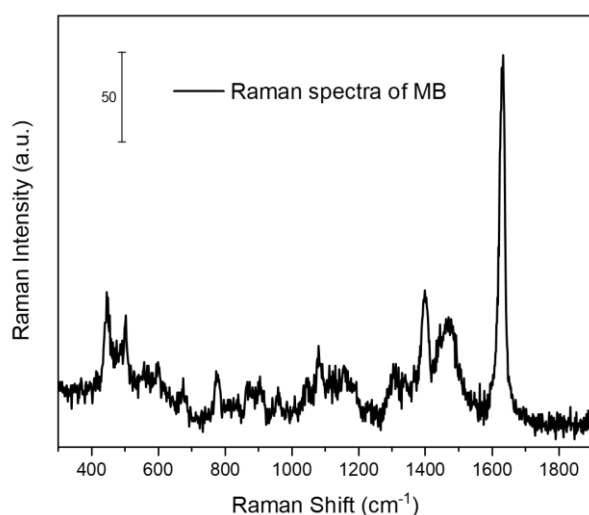


**Figure 7.** Raman spectra of MB (100 mM, in DI water/ methanol (8:2 vol%)).

Calculation of Analytical enhancement factor (AEF):

$$I_{SERS} = 4821 \text{ counts}; I_{RS} = 219 \text{ counts}; c_{SERS} = 10\text{ }\mu\text{M} \text{ and } c_{RS} = 100\text{ mM}$$

$$AEF = 2.2 \times 10^5$$

## S12. Mechanism of the photocatalysis

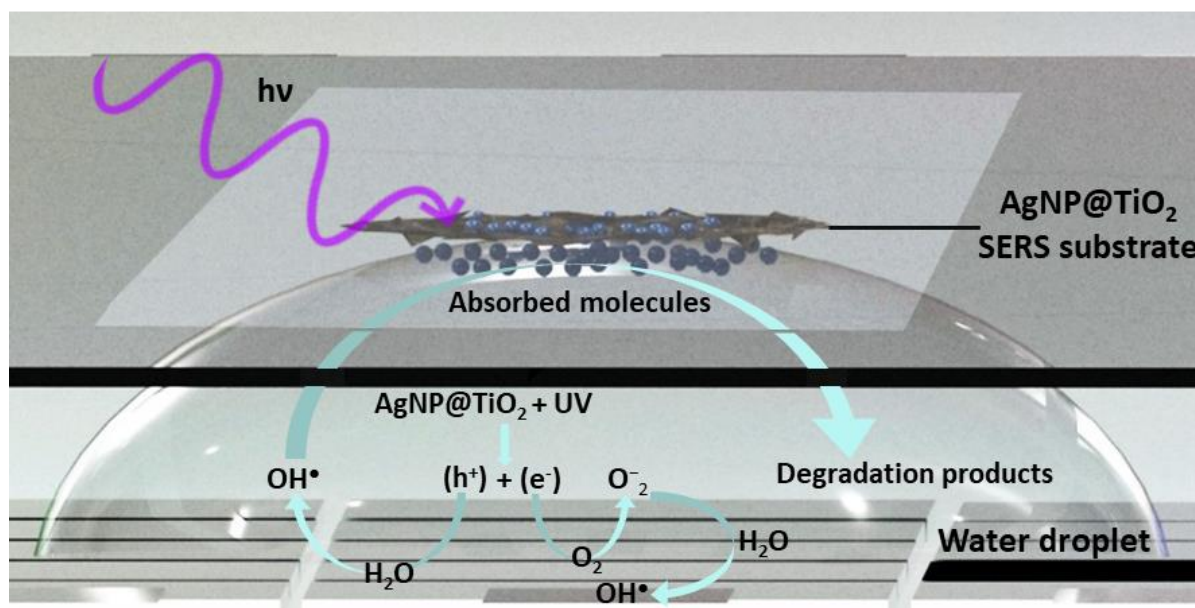


**Figure 8.** Schematic showing the photocatalysis process inside the digital microfluidics chip.

This mechanism can be explained by the fact that the AgNP integrated into the TiO<sub>2</sub> thin film function as an electron trap.<sup>12</sup> During the UV irradiation process, the electrons in the TiO<sub>2</sub> are excited from the valance band to the conduction band. Due to silver having a lower work function compared to TiO<sub>2</sub>, silver accepts these electrons transferred from the TiO<sub>2</sub> while the holes remain in the TiO<sub>2</sub>.<sup>13</sup> This leads to the separation of the photogenerated electron-hole pairs, which is essential for the photocatalytic degradation process. As a result, the recombination of the electron-hole pair is significantly suppressed. The holes are captured by H<sub>2</sub>O, forming hydroxyl (OH<sup>•</sup>) radical and the electrons are transferred to oxygen (O<sub>2</sub>) forming superoxides (O<sub>2</sub><sup>-•</sup>).<sup>1</sup> These active oxidative species react with the adsorbed analyte molecules decomposing them into more minor inorganic compounds<sup>1</sup>. These inorganic compounds are then washed away from the SERS substrate by multiple on-chip DMF-activated cleaning steps.

### S13. Control experiment with cleaning solution

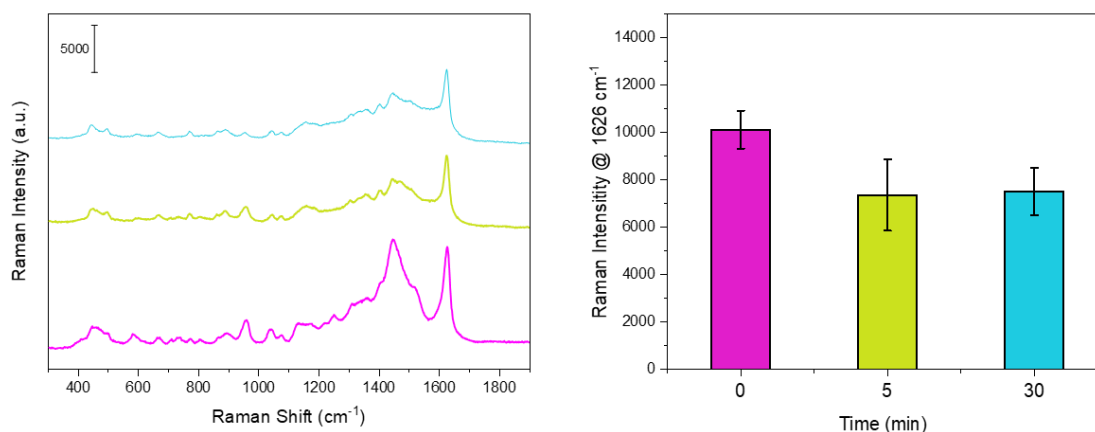


**Figure 9.** Results of the control experiment with cleaning solution, Left: SERS spectra with normalized intensity, Right: bar diagram of band intensities @ 1626 cm<sup>-1</sup> after certain time, only exposed to cleaning (no additional UV irradiation), Magenta: Contaminated SERS substrate directly before exposed to cleaning solution, Yellow: Contaminated SERS substrate after 5 min exposed to cleaning solution, Cyan: Contaminated SERS substrate after 30 min exposed to cleaning solution

To validate our DMF integrated SERS substrate regeneration approach, control experiments were performed. In this experiment, it was examined whether the cleaning solution itself had any influence on the recycling process. The experimental steps followed the same process as in the main regeneration experiment, with the exception that now the UV irradiation was not applied. For this purpose, the cleaning solution was actuated under the contaminated (with MB) SERS substrate and no additional UV irradiation was applied. Just like the standard cleaning process of the main experiment the cleaning solution was exchanged every 5 min, but this time over a longer period of 30 min in total. As a result, no significant cleaning of the contaminated SERS substrate can be observed as the SERS signal for MB is still visible after 30 min. The slight decrease in the band intensity after the first measuring interval can be explained due to a small rinsing effect.

#### S14. Control experiment with UV irradiation

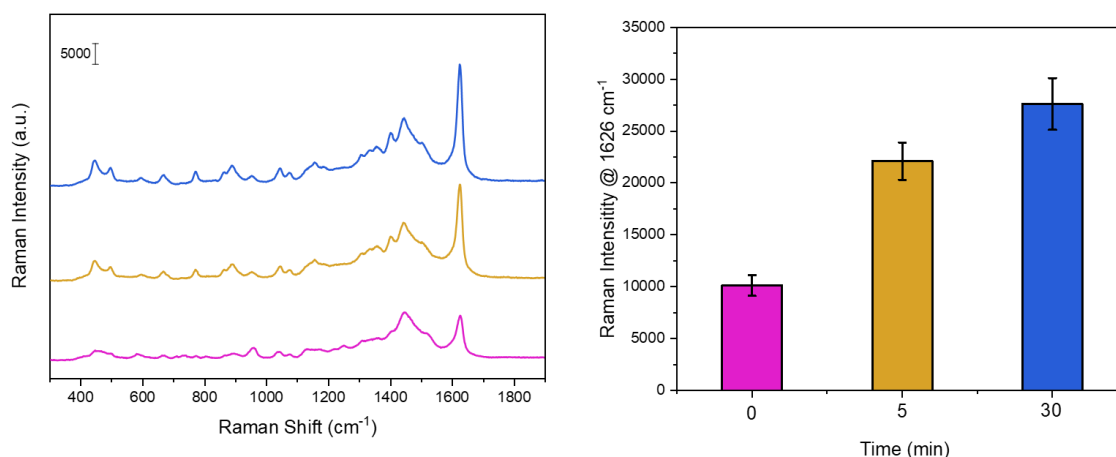


**Figure 10.** Results of the control experiment with UV irradiation, Left: SERS spectra with normalized intensity, Right: bar diagram of band intensities @ 1626 cm<sup>-1</sup> after certain time only exposed to UV light (no cleaning solution), Magenta: Contaminated SERS substrate directly before exposed to UV light, Ochre: Contaminated SERS substrate after 5 min exposed to UV light, Blue: Contaminated SERS substrate after 30 min exposed to UV light

During the second experiment, the cleaning was adjusted in the way, that the contaminated SERS spot is only irradiated by UV light and no cleaning solution was in touch with the contaminated SERS substrate. One irradiation sequence takes 5 min over a period of 30 min in total. No reduction of signal intensity can be observed. Instead the signal intensity grows with the ongoing time of irradiation. Presumably this is due to further evaporation of remaining solvent on the surface of the contaminated SERS substrate.

### S15. Comparison between on-chip vs off-chip AgNP@TiO<sub>2</sub> SERS substrate

	Automation	Substrate Size	Volume of analyte	Regeneration time	Number of cycle	Analyte
Digital microfluidics integrated AgNP@TiO <sub>2</sub>	Yes	1 mm (diameter)	Droplet (1-4 μl)	15-25 min	5	MB, MG malathion
Porous Ag/TiO <sub>2</sub> Composite film [1]	No	15 × 15 mm	NA	NA	4	CV
Ag-deposited TiO <sub>2</sub> flower-like nanomaterial (FLNM) [14]	No	15 × 15 mm	soaked in analyte solution bath for 3h	60 min	3	MG
Ag Nanorods Coated with Ultrathin TiO <sub>2</sub> Shells [13]	No	NA	soaked in analyte solution bath for 30 min	20 min	4-5	CV, MB

**Table 1.** Comparison between on-chip vs off-chip AgNP@TiO<sub>2</sub> SERS substrate.

### S16. Droplet movement speed

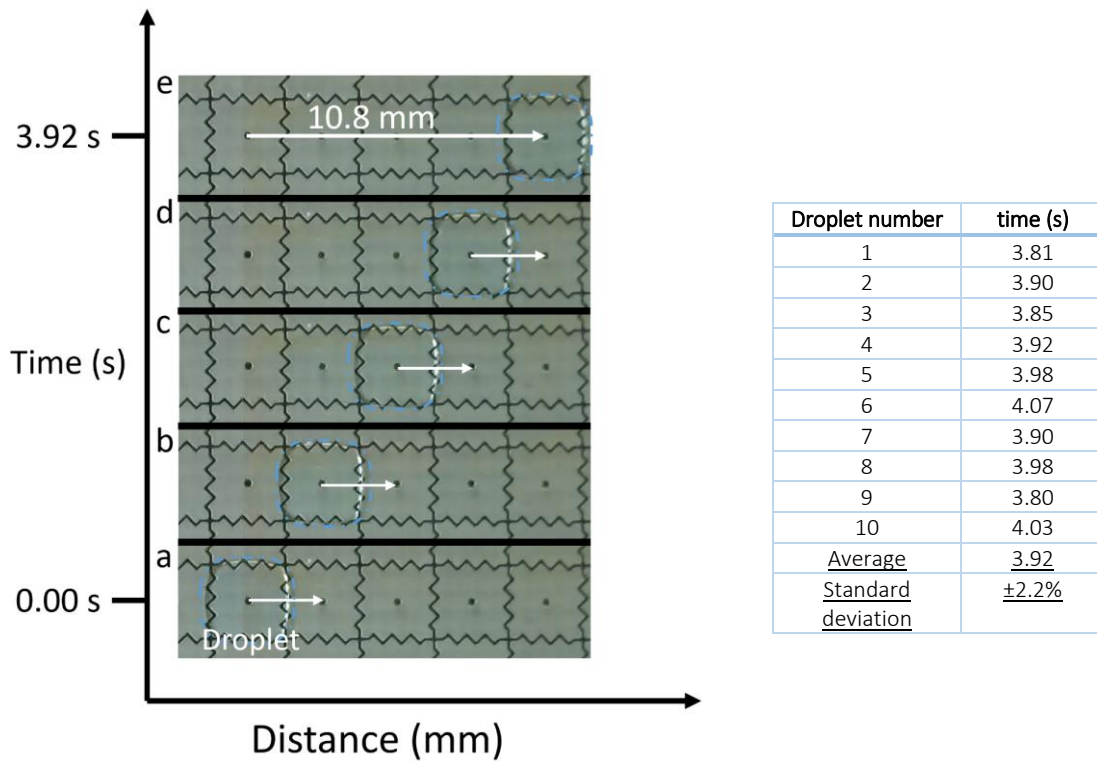


**Figure 11.** (a-e) Droplet movement inside the DMF chip from one electrode to the adjacent ones. Table showing the time taken for 10 droplets to travel a distance of 10.8 mm.

Voltage → 280 V

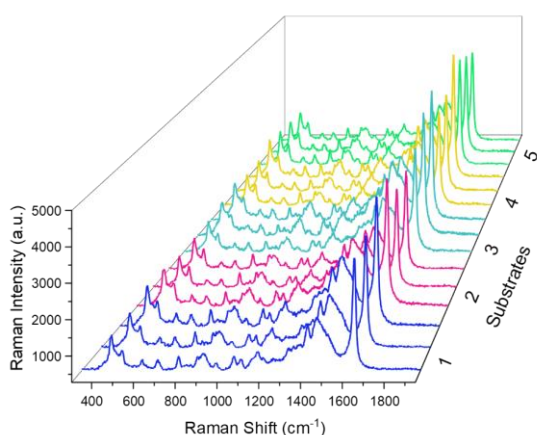
Frequency → 1.0 kHz

Distance →  $d_{ae} = 10.8$  mm

Time →  $t_{ae} = 3.92$  s ( $\pm 2.2\%$ )

**Speed of droplet** →  $V_T = d_{ae} / t_{ae} = 2.75$  mm/s ( $\pm 2.2\%$ )

## S17. SERS substrate reproducibility



	Spot1	Spot2	Spot3	Average	Std Dev	RSD
Substrate 1	3416	3512	4121	3683	312.18	8.476
Substrate 2	4173	3357	3436	3655.333	367.46	10.052
Substrate 3	3702	4421	4758	4293.667	440.41	10.257
Substrate 4	3593	3764	4821	4059.333	543.09	13.378
Substrate 5	4257	3991	3743	3997	209.88	5.251
			Mean	3937.667	374.61	9.513

**Figure 12.** SERS spectra for Substrate-to-substrate variation for five SERS substrates measured at 3 different spot within a particular substrate. The peak at  $1628\text{ cm}^{-1}$  in the SERS spectrum was used to calculate the mean intensity. Table showing the calculation for the average intensities, standard deviation and the RSD.

## S18. Limit of detection (LOD)

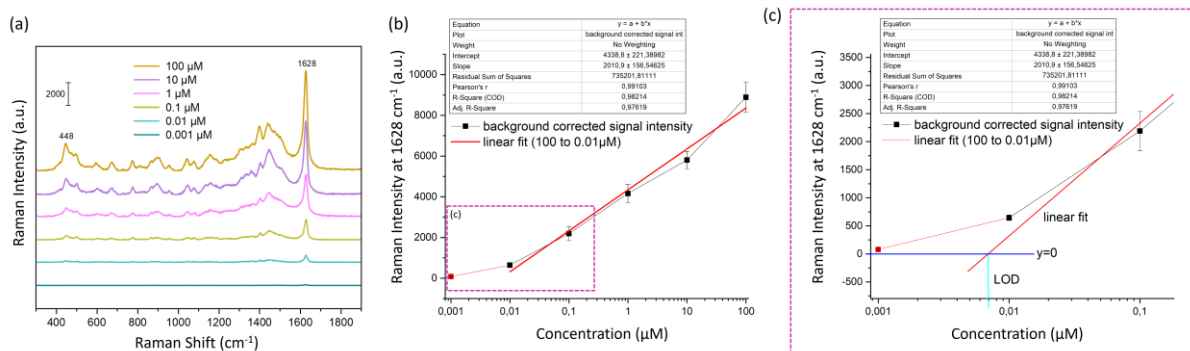


**Figure 13.** (a) Concentration-dependent SERS spectra of methylene blue on DMF integrated AgNP@TiO<sub>2</sub>. Laser wavelength: 532 nm, exposure time 1 sec, number of accumulation 1. (b-c) The fitting curve of SERS intensity versus concentration plots at  $1628\text{ cm}^{-1}$  for determining the limit of detection.

Calculation of the LOD:

Formula of linear fit:  $y = a + b * x$

$y = 0$ ,

$0 = a + b * x$ ,

$x = -a/b$ ;

Linear fit	a	b	y	x (in $1*10^x$ )	x (linear)
100 to 0.01 $\mu\text{M}$	4338.8	2010.9	0	-2.158	0.00696

Therefore, it can be determined that the limit of detection is **0.00696  $\mu\text{M}$  or 6.96 nM**.

### S19. Detection-recycling cycles for malathion

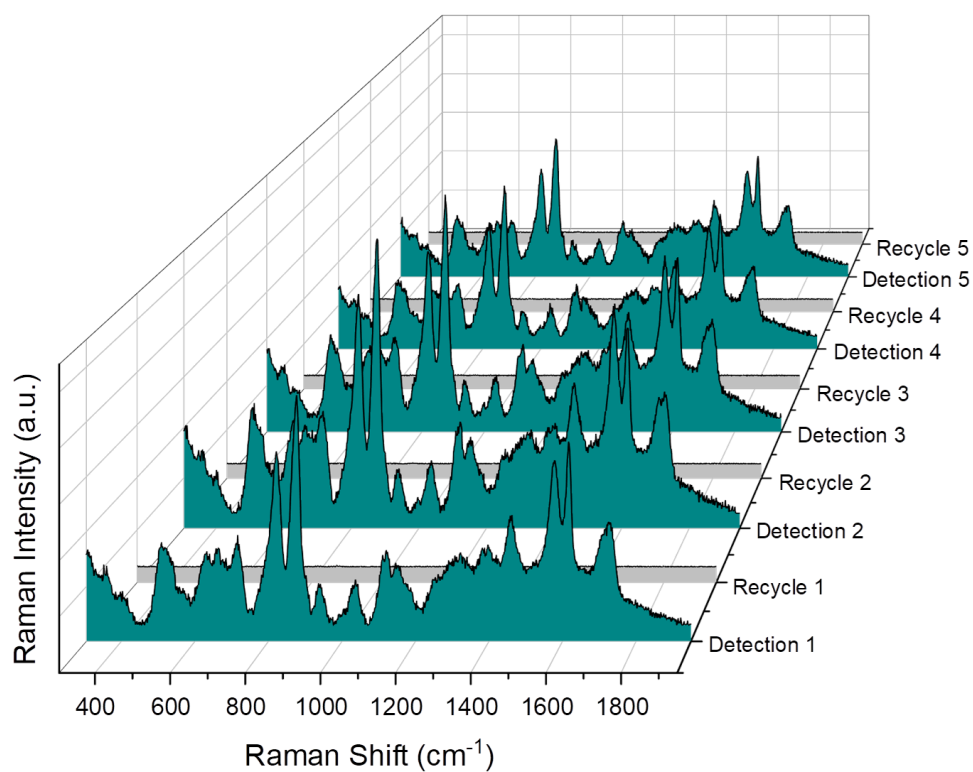


**Figure 14.** SERS spectra of malathion (50  $\mu\text{M}$ ) adsorbed onto the DMF integrated AgNP@TiO<sub>2</sub> SERS substrate showing “detection-recycling” cycles.

## S20. Trade-off between droplet movement versus SERS detection

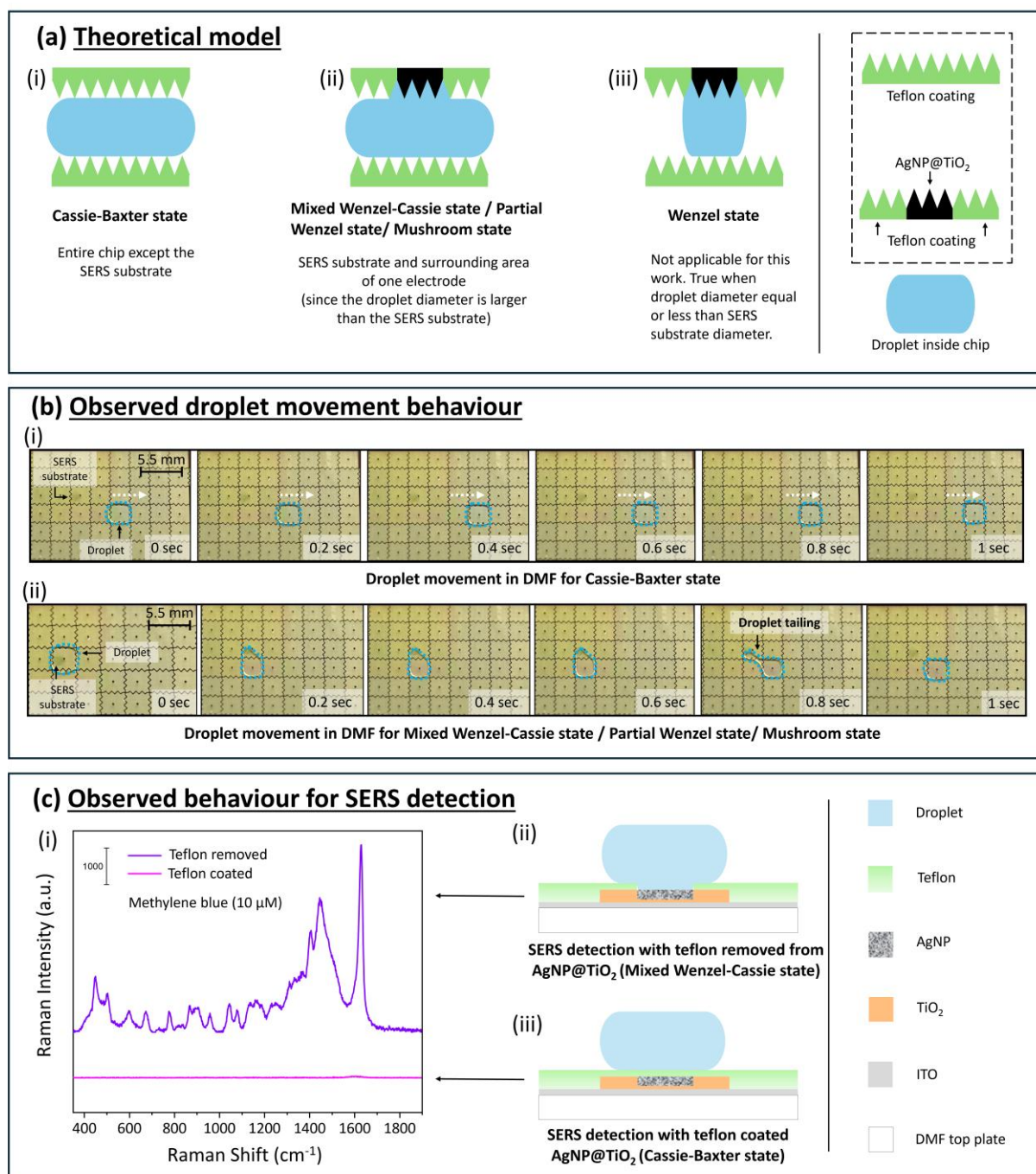


**Figure 15.** (a) Theoretical models for different hydrophobic/hydrophilic surface-droplet interaction inside the DMF chip. (b) Frames from video (export frame rate: 5 images per second) for the observed droplet movement in DMF for Cassie-Baxter-state and mixed Wenzel-Cassie state. (c) SERS spectra obtained for Cassie-Baxter-state and mixed Wenzel-Cassie state. Analyte: methylene blue (10 μM), Laser parameter: wavelength- 532 nm, power- 13 mW, exposure time 1 sec, number of accumulation-1. All spectra were acquired within 5 min of analyte deposition.

Figure 15 illustrates the relation between DMF-droplet movement in regards to surface hydrophobicity and SERS activity. In Figure 15(a), theoretical models depict various hydrophobic/hydrophilic interactions between the surface and the droplet within the DMF chip.

Fig.15(a), (i): The droplet is in a classic Cassie-Baxter state with high hydrophobicity (represented by green spikes) across the entire surface of the chip, except for the SERS substrate. In this scenario, the droplet size is irrelevant.

Fig.15 (a), (ii): When the droplet inside the chip comes into contact with the SERS substrate, it transitions into a mixed Wenzel-Cassie state/Partial Wenzel state. This is because the droplet diameter is larger than the SERS substrate diameter. Consequently, the entire droplet interacts with both the hydrophilic area (SERS substrate, black spikes) and the surrounding highly hydrophobic area (Teflon-coated glass within one electrode area, green spikes).

Fig.15(a), (iii): Shows a droplet in the classic Wenzel state, where the droplet diameter is equal or smaller than the hydrophilic area, resulting in purely hydrophilic interactions. This scenario is not applicable for this work.

This theory is experimentally explained in Fig 15(b), which shows the observed droplet movement for the models relevant to this study. Frames from ESI video 1 were captured to analyze the droplet movements inside the DMF chip (export frame rate: 5 images per second, Adapter software, Macroplant LLC, USA).

Fig. 15(b), (i): Shows the observed droplet movement for Cassie-Baxter state, where no droplet retention is observed (for the given frame rate), due to the uniform hydrophobic surface.

Fig.15(b), (ii): In the mixed Wenzel-Cassie state, droplet tailing occurs due to hydrophilic interactions at specific spots (SERS-active substrates), while the surrounding area remains hydrophobic. This interaction results in a "sticky" behaviour of the droplet towards the SERS spot, confirming the presence of the Wenzel-Cassie state. Because the droplet size is larger than the SERS substrate (Wenzel-Cassie state), the droplet can be moved further away from the hydrophilic spot (fig.15(b), (ii) frame at 1 sec), a scenario that wouldn't be possible in a fully Wenzel state.

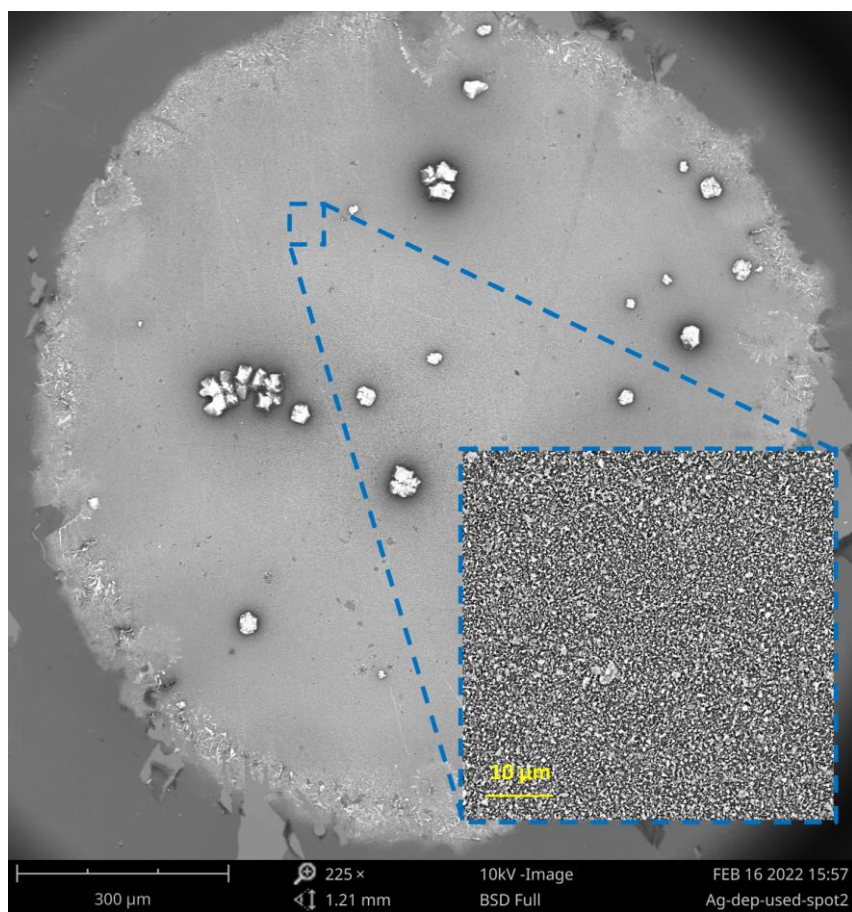
The theory is further elucidated experimentally in Fig.15(c), which shows the observed SERS signal for the models. Fig.15(c), (i) compares the SERS activity of AgNP@TiO<sub>2</sub> spots in mixed Wenzel-Cassie and Cassie-Baxter states.

Fig.15(c), (i & ii): The violet SERS spectrum indicates an acceptable signal for the dehydrophobised (hydrophilic) condition (or mixed Wenzel-Cassie state) and therefore active SERS spot.

Fig. 15(c), (i & iii): The pink SERS-spectrum shows no signals for the hydrophobic condition (Cassie-Baxter state) and thereby inactive SERS-spot.

Therefore, dehydrophobisation by the removal of Teflon precursor from the SERS-spot, is necessary to achieve SERS-activity.

S21. SEM image of the SERS substrate after five cycle



**Figure 16.** SEM image of the DMF integrated SERS substrate acquired after 5 cycles showing the surface morphology of AgNP@TiO<sub>2</sub>.

## References

- [1] Z. Zhang, J. Yu, J. Yang, X. Lv, T. Wang, *Applied Surface Science* 2015, 359, 853-859.
- [2] H. E. Swanson, R. K. Fuyat, G. M. Ugrinic, *US National Bureau of Standards Circular*, **1955** 539, 4, 1-75.
- [3] M. Horn, C. F. Schwerdtfeger, E. P. Meagher, *Z. Kristallogr.*, **1972**, 136 273-281.
- [4] W. H. Baur, A. A. Khan, *Acta Cryst. B*, **1971**, 27, 2133-2139.
- [5] E. P. Meagher, G. A. Lager, *Can. Mineral.*, **1979**, 17, 77-85.
- [6] H. M. Rietveld, *J. Appl. Crystallogr.* **1969**, 2, 65-71.
- [7] *Topas*, version 5.0.0.13; Bruker AXS GmbH, **2014**.
- [8] Maria D. P. R. Torres, *Int.J.Mol.Sci.*, **2014**, 15, 19239-19252.
- [9] Wei Zhang, *J.Photochem.Photobio. A: Chem.*, **2021**, 406, 112987.
- [10] Chunying Li, *Food Control*, **2016**, 65, 99-105.
- [11] Le Ru, E. C.; Blackie, E.; Meyer, M.; Etchegoin, P. G. *J. Phys. Chem. C* **2007**, 111 (37), 13794-13803.
- [12] H. Atta ul, S. Muhammad, K. Samreen Gul and I. Muhammad, in *Titanium Dioxide*, ed. A. Hafiz Muhammad, IntechOpen, Rijeka, 2021, DOI: 10.5772/intechopen.99598, p. Ch. 4.
- [13] L. Ma, Y. Huang, M. Hou, Z. Xie and Z. Zhang, *Sci. Rep.*, 2015, 5, 15442.
- [14] W. Yang, J. Tang, Q. Ou, X. Yan, L. Liu, and Y. Liu, *ACS Omega*. 2021 6 (41), 27271-27278